OPTICS

Coupling light to a nuclear spin gas with a two-photon linewidth of five millihertz

Or Katz[1,2]*, Roy Shaham[1,2], Ofer Firstenberg[1†]

Nuclear spins of noble gases feature extremely long coherence times but are inaccessible to optical photons. Here, we realize a coherent interface between light and noble-gas spins that is mediated by alkali atoms. We demonstrate the optical excitation of the noble-gas spins and observe the coherent back action on the light in the form of high-contrast two-photon spectra. We report on a record two-photon linewidth of 5 ± 0.7 mHz above room temperature, corresponding to a 1-min coherence time. This experiment provides a demonstration of coherent bidirectional coupling between light and noble-gas spins, rendering their long-lived spin coherence accessible for manipulations in the optical domain.

INTRODUCTION

The coupling of light to atomic spins is a principal tool in quantum information processing using photons (*1*–*4*) and in precision optical spectroscopy, enabling determination of atomic structure (*5*, *6*), time and frequency standards (*7*), and laboratory searches of new physics (*8*). The performance of these applications depends on the coherence time of the spins and on the efficiency with which they couple to light. In dense atomic gases, light can couple efficiently to the collective atomic spin of the ensemble (*9*). However, at room temperature and above, this collective spin is prone to decoherence due to interactions of the atoms with the environment and due to motional dephasing, which typically limit the coherence time to 10 to 100 ms (*10*–*14*). Alkali vapor in antirelaxation-coated cells can reach coherence times as long as 1 min (*15*–*18*) and is successfully used in quantum-optics applications (*9*), but the high-quality coatings degrade at elevated temperatures and thus limit the alkali densities.

Odd isotopes of noble gases, such as ^{3}He, have a nonzero spin in their nuclei. The nuclear spin is protected by the full electronic shells and therefore exhibits extraordinary long coherence times, possibly many hours. This corresponds to a narrow nuclear magnetic resonance (NMR) that is used for precision sensing (*19*, *20*), medical imaging (*21*), and searches for new physics (*22*–*25*). As noble gases are transparent to light from infrared to ultraviolet, the preparation and monitoring of their nuclear spins usually rely on collisions with another spin gas (*26*, *27*). Noble-gas NMR sensors use spin-exchange collisions with alkali atoms. Because alkali spins do couple to light, the pickup of the NMR signal can be done optically, and, in this way, narrow spectra and long-lived spin precession signals are routinely obtained (*28*–*31*). Yet, various quantum optics applications require an efficient bidirectional coupling between light and noble-gas spins (*32*–*36*). Such coupling, corresponding to a resonant optical excitation of the long-lived nuclear spins, has never been realized.

Here, we realize a coherent bidirection coupling between light and noble-gas spins, mediated by alkali spins. We observe a substantial attenuation of the optical signal at the nuclear magnetic resonance of the noble gas, accompanied by excitation of noble-gas spin coherence. We control the contrast and width of the spectroscopic lines with an external magnetic field, realizing narrow linewidths down to 5 ± 0.7 mHz. The efficient collective coupling to the noble-gas spins, enabled by the high alkali vapor density, is reflected in the high spectroscopic contrast and in a direct measurement of the transverse spin excitation of the noble gas. This interface between photons and long-lived nuclear spins opens routes to various applications in precision sensing and quantum information science, including generation of entanglement and quantum memories with unprecedented lifetimes (*32*, *35*).

RESULTS

To generate a bidirectional coupling between light and noble-gas spins, we use a mixture of gaseous ^{3}He (nuclear spin $R = {}^1/_2$) and potassium (electron spin $^1/_2$ and nuclear spin $^3/_2$), enclosed in a spherical glass cell at 187°C, as shown in Fig. 1. Light directly interacts only with the potassium atoms, whose spin is optically accessible owing to their electronic orbital transitions in the infrared and to their strong spin-orbit and hyperfine couplings. We optically pump the potassium spin **F** along $\hat{z}$, which, in turn, continuously polarizes the helium nuclear spin **R** via spin-exchange collisions (*26*). A constant magnetic field $B\hat{z}$ controls the Larmor frequencies ω_a and ω_b of the alkali and noble-gas spins, which are also affected by light shifts and by the equivalent magnetic field (EMF) produced by the polarized spins.

The light field interacting with the spins is a superposition of a signal field and an auxiliary control field, copropagating in the $\hat{x}$ direction. Both fields are tuned near the potassium D_1 transition at 770 nm, which appears as a single optical line of width $2\gamma_e = 25$ GHz due to pressure broadening by the ^{3}He at 1500 torr. The fields are detuned by $\delta_e \approx 40\gamma_e$ from this line, so their attenuation via scattering is suppressed. The control is linearly polarized parallel to the magnetic field, while the weak signal is linearly polarized in the transverse direction $\hat{y}$.

The optical frequency of the signal field differs from that of the control field by a tunable frequency ω, generated in our experiment by two acousto-optic modulators. This frequency difference leads to a temporal polarization modulation of the combined field, which can be represented as a precession of the optical Stokes vector, as

[1]Department of Physics of Complex Systems, Weizmann Institute of Science, 7610001 Rehovot, Israel. [2]Rafael Ltd, IL-31021 Haifa, Israel.
*Present address: Department of Electrical and Computer Engineering, Duke University, Durham, NC 27708, USA.
†Corresponding author. Email: ofer.firstenberg@weizmann.ac.il

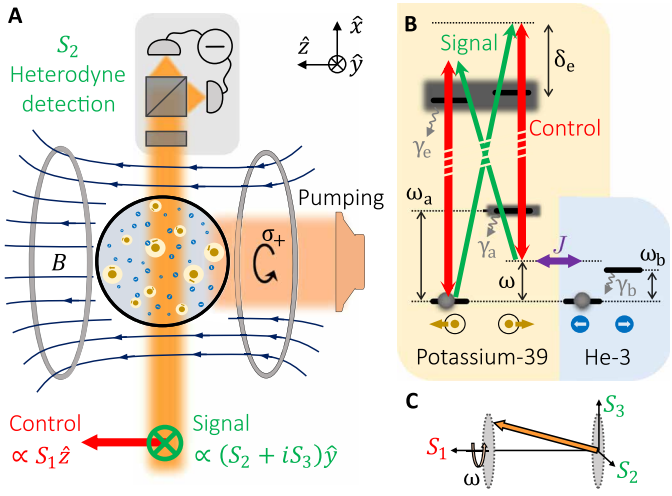

Fig. 1. Coupling light to noble-gas nuclear spins. (**A**) Experimental setup and (**B**) level diagram of the optical and spin-exchange couplings. A gaseous mixture of potassium (beige) and helium-3 (blue) atoms is contained in a spherical glass cell. The potassium spins are polarized along the $\hat{z}$ direction by absorption of circularly polarized pumping light. The helium spins are polarized by collisions with potassium atoms. The incoming light comprises a $\hat{z}$-polarized control field (quadrature S_1 in the Stokes representation) and a $\hat{y}$-polarized signal field (quadratures S_2 and S_3). It interacts with the potassium spins via a two-photon process and is measured by heterodyne detection. Both fields are far-detuned by $|\delta_e| \gg \gamma_e$ from the potassium optical transitions of width γ_e, but the signal field differs from the control field by a small frequency ω, leading to precession in the Stokes vector representation (**C**). The alkali and noble-gas spins are coherently coupled by spin exchange at a rate J and decohere at rates $\gamma_a \gg \gamma_b$. A magnetic field $B\hat{z}$ determines the Larmor frequencies ω_a and ω_b of the two spin excitations, thus controlling their mutual coupling and their detunings $\delta_a = \omega - \omega_a$ and $\delta_b = \omega - \omega_b$ from the optical modulation frequency.

shown in Fig. 1C. In this representation, the optical signal resides in the oscillating components S_2 and S_3. We perform heterodyne detection before and after the cell using two pairs of differential photodetectors to obtain the incoming and outgoing signal components $S_2^{\text{in}}(\omega)$ and $S_2^{\text{out}}(\omega)$ in a frame rotating at the modulation frequency ω. Technically, this is done by extracting the amplitude and phase shift of the measured harmonic oscillations at the frequency ω. This spectroscopic technique, in which light efficiently couples to the orientation moment of the alkali spins irrespectively of the width of their optical transitions, is a special variation of the nonlinear Voigt effect (*37*) that is applicable even at high buffer-gas pressures. Further details on the experimental configuration and schemes are given in Materials and Methods.

We begin our investigation in the regime $\omega_a \gg \omega_b$, where the magnetic resonance of the noble-gas spins is detuned away from that of the alkali spins. In this regime, the noble-gas resonance is nested in the tail of the alkali resonance, much like a Raman line that is nested in the tail of an optical line. If $|\omega_b - \omega_a| \gg \gamma_a$, where γ_a is the alkali spin decoherence rate, then, when we tune the optical field near the noble-gas resonance $\omega \approx \omega_b$, the alkali spins act as an intermediate system that is only weakly excited. Despite the large detuning from the alkali resonance, we observe a substantial change in the signal field due to the nonlinear Voigt effect around the noble-gas resonance. We observe a response in both the transmission $|S_2^{\text{out}}(\omega)/S_2^{\text{in}}(\omega)|^2$ and phase $\varphi = \arg[S_2^{\text{out}}(\omega)/S_2^{\text{in}}(\omega)]$ of the S_2 light quadrature, as shown in Fig. 2 (A and B) for $B = 6.1$ mG ($|\omega_b - \omega_a| \approx 43\gamma_a$). We fit the sharp spectral line in Fig. 2A to a Lorentzian shape and find a maximal attenuation (contrast) of $\mathcal{C} = (53 \pm 3)\%$ and a full width of $2\gamma = 10.5 \pm 1.4$ mHz. The observed line center ($\Delta = 0$ in Fig. 2) differs from the bare resonance $\omega = \omega_b$ by <50 mHz predominantly due to NMR shifts induced by the alkali spin-exchange field. The same parameters γ and $\mathcal{C}$ fit as well the phase shift across the resonance, presented in Fig. 2B, as calculated from a theoretical model (see Materials and Methods).

The resonant interaction of the noble-gas spins with light also sets the spins in motion and subjects them to coherent precession transversely to the magnetic field. To demonstrate this optical excitation, we send a long signal pulse (duration $T = 3/\gamma$) and, subsequently, while keeping the control field on, monitor the precession of the noble-gas spins using the polarization rotation of the control field. The readout $R_\perp(t)$, proportional predominantly to the x projection of the noble-gas spin $\mathbf{R}$, oscillates at the frequency ω_b, as shown in Fig. 2D (see Materials and Methods). We denote by $R_{0\perp}$ the amplitude of these oscillations and present $|R_{0\perp}|^2$ as a function of the optical signal frequency in Fig. 2C. As expected, the response of the spins to the optical excitation follows a narrow Lorentzian profile of linewidth 2γ.

The sharp variation of the optical susceptibility and the excitation of spin coherence near the resonance of the noble-gas spins are evidence for the emergent interaction between noble-gas spins and light. We now turn to model this interaction and study its dependence on the applied magnetic field. The polarized alkali atoms, mediating this interaction, couple to the optical signal via the so-called Faraday Hamiltonian (*9*) and couple magnetically to the noble-gas spins. The magnetic coupling is dominated by frequent spin-exchange collisions, whose accumulative effect leads to asymmetric shifts of the Larmor frequencies and to coherent exchange between the transverse components of the two spins (in the xy plane) at a rate J (*38*). See Materials and Methods for the detailed model.

The evolution under the joint optical and exchange interactions can be described in the following picture. The oscillating quadrature S_3 of the light field (pertaining to circular polarization) drives the transverse alkali spin component F_y at the frequency ω, via a light-induced shift. The transverse alkali spin components (F_x, F_y) couple to the transverse noble-gas spin components (R_x, R_y) by the exchange interaction. Therefore, the noble-gas spin can be resonantly excited when ω is tuned near its resonance frequency ω_b. Because the process is detuned from the alkali resonance frequency ω_a, the alkali spin effectively hybridizes with the noble-gas spin and adiabatically follows the noble-gas spin precession (*39*). As a back action, the precessing alkali spin—specifically its oscillating component F_x along the optical axis—rotates the light polarization and therefore changes the amplitude and phase of $S_2(\omega)$.

Using this picture, we theoretically calculate in Materials and Methods the output light quadrature $S_2^{\text{out}}(\omega)$. When the alkali spin resonance is far detuned, i.e., when $|\delta_a| \gg \gamma_a$, where $\delta_a \equiv \omega - \omega_a$, we find that $S_2^{\text{out}}(\omega)$ around the noble-gas resonance is an inverted complex Lorentzian with a half width

$$\gamma = \gamma_b + \frac{J^2}{\delta_a^2 + \gamma_a^2}\gamma_a \quad (1)$$

The first term γ_b is the bare decoherence rate of the noble-gas spins. The second term is due to the hybridization of the noble-gas

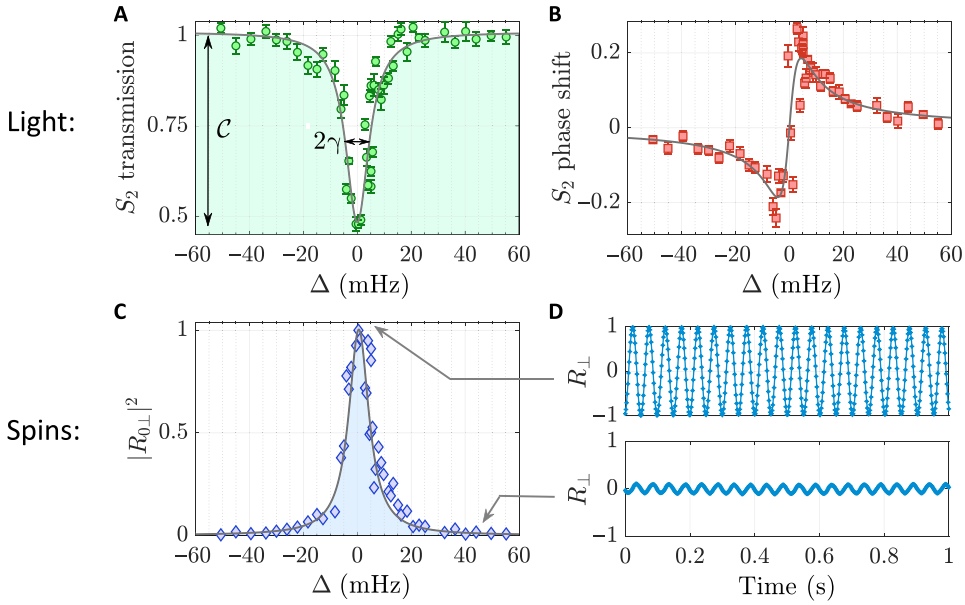

Fig. 2. Optical spectroscopy and excitation of helium-3 spins. (**A**) Transmission of the S_2 quadrature of the signal light versus the signal frequency detuning Δ from the observed resonance. The sharp spectral line, due to a two-photon process, is obtained when the frequency difference ω between the signal and control fields approaches the nuclear magnetic resonance of the noble gas $\omega_b = 19.88$ Hz (here, $B = 6.1$ mG and $\omega_a = 2.2$ kHz). A Lorentzian profile (solid line) fits the data well, providing a narrow linewidth of $2\gamma = 10.5 \pm 1.4$ mHz and a contrast of $\mathcal{C} = 53 \pm 3\%$. (**B**) Phase shift of the S_2 quadrature of the signal. The theory (solid line, see Eq. 9) agrees with the data using the same γ and $\mathcal{C}$ and no other fit parameters. (**C** and **D**) Optical excitation of noble-gas spin coherence. (C) On resonance, the light field excites the noble-gas spins, which steadily precess with amplitude R_{0x} normalized to unity at maximal value (see Eq. 11). A Lorentzian profile with linewidth 2γ (solid line) fits the data well. (**D**) Measured precession signals on and off resonance. In (A) and (B), each data point is obtained from fitting a single heterodyne measurement to a shifted harmonic signal (bars represent the fit confidence interval of 95%). Error bars in (C) are below the marker size.

and alkali spins, with the former inheriting a fraction $J^2/(\delta_a^2 + \gamma_a^2)$ of the alkali decoherence rate. This fraction is primarily set by the magnetic field via $\delta_a(B)$. We furthermore derive the contrast $\mathcal{C}$ of the spectral line (the maximal attenuation) and find that it, as well, decreases with increasing $|\delta_a|$, as the coupling mediated by the alkali spins weakens (see Eqs. 8 and 10). It is therefore expected that decreasing the magnetic field will increase the contrast, broaden the spectral line, and enhance the spin precession signal.

To verify the model, we measure optical spectra for varying magnetic fields and present the extracted linewidth and contrast in Fig. 3. We fit the data to our model and find an excellent agreement with the dependence on the magnetic field, for $J = 14 \pm 0.4$ Hz and $2\gamma_b = 4.8 \pm 1$ mHz, the latter mainly limited in our setup by nonuniformity of the EMF of the gases over the cell volume. The alkali parameters $\gamma_a = 51 \pm 3$ Hz and $\delta_a(B)$ are calibrated independently (see Materials and Methods). We obtain the narrowest line for $B = 10.7$ mG, with a width of $2\gamma = 5 \pm 0.7$ mHz that approaches the bare decoherence rate $2\gamma_b$. We note that the basic constraints that connect B to δ_a and determine the degree of coupling could potentially be circumvented by modulating the magnetic field near the alkali spin resonance frequency (*40*).

Last, we use a magnetic pulse excitation to independently measure the transverse relaxation rate of the noble-gas spins in the absence of a signal field. The data, presented in Fig. 3A (diamonds), attest that the noble-gas decoherence rate is insensitive to the amplitude of the signal.

DISCUSSION

It is insightful to compare the magneto-optical response we use in this study with the response used in noble-gas NMR sensors, such as NMR gyroscopes (*20*, *41*). While the former is linear in the signal field and nonlinear in the control field, i.e., a $\chi^{(3)}$ process (nonlinear susceptibility), the latter is linear in the control field only, which is a $\chi^{(1)}$ process (linear susceptibility) (*37*, *42*, *43*). Therefore in NMR sensors, the rotation of the control field appears as an additive (source) term in the outgoing signal field, which is independent of the incoming signal amplitude. In contrast, the $\chi^{(3)}$ process used in this work produces a homogeneous term in the propagation equations of the signal. This homogeneous term, corresponding to a linear coupling between the signal and the spins, is desired for quantum optics applications. It indicates that the signal field excites the spins, as opposed to NMR sensors, where the spins are excited by an external perturbation (namely, rotation or magnetic field). High efficiency of the bidirectional interface requires a large bidirectional coupling rate $J = \sqrt{J_a J_b}$, defined in terms of the unidirectional coupling rates J_a and J_b (see Eq. 3 in Materials and Methods), which corresponds to maximizing the spin-exchange fields of both gases. In contrast, the unidirectional operation of NMR sensors relies only on J_a, which depends solely on the spin-exchange field of the noble gas. A bidirectional optical interface to noble-gas spins can be used to couple noble-gas spins to distant objects, such as done in hybrid optomechanical-atomic-spin systems (*44*–*46*).

Quantum memories, in particular, require several extensions to our scheme, which are readily available. First, quantum memories necessitate the coherent mapping of both quadratures of the signal field on the spins (*9*), whereas, in this work, only one quadrature couples coherently to the noble-gas spins. To realize a complete mapping in the presence of high noble-gas pressure, the so-called double-pass interaction can be used, by sending the light beam twice through

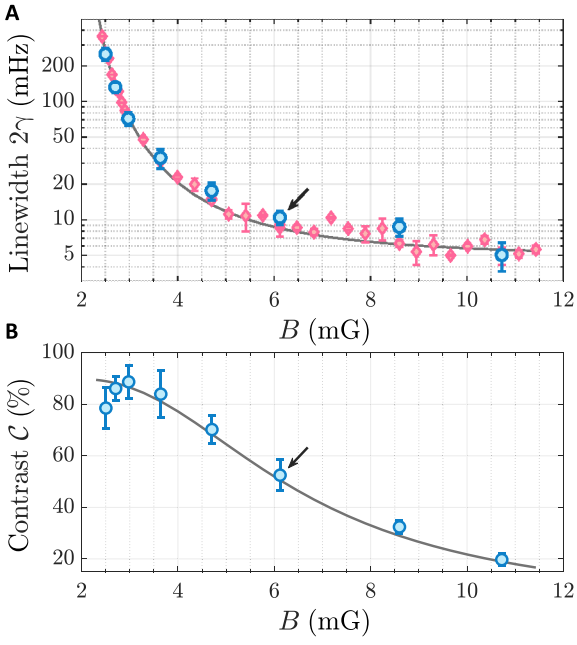

Fig. 3. Magnetic control of the optical spectral line. (**A**) Narrowing of the line and (**B**) decrease of the line contrast with increasing magnetic field. Circles are spectroscopic data and lines are the theoretical model, which describes the hybridization of the noble-gas and alkali spins. Stronger hybridization (low magnetic field) leads to stronger optical response at the noble-gas resonance on the expense of faster relaxation of the hybridized spin (dominated by the alkali relaxation). Black arrows indicate the measurements presented in Fig. 2. In (A), the spectroscopically measured linewidths agree with independent transient measurements of the relaxation rate of the noble-gas spins (diamonds). The measured linewidth at $B = 10.7$ mG is $2\gamma = 5 \pm 0.7$ mHz, approaching the bare noble-gas decoherence rate in our setup. Error bars represent a confidence interval of 95%.

the cell (*47*, *48*). Second, quantum memories require a high bandwidth of the mapping process compared to the decoherence rate of the spins. A large time-bandwidth product usually requires temporal variations of external classical fields. Variations of the magnetic and control fields can be done during the reading and writing processes to increase the bandwidth and, during the memory time, to decouple the noble-gas spins from the alkali and consequently reduce its decoherence rate down to γ_b (*35*, *36*).

In summary, we realize an efficient bidirectional coupling between noble-gas spins and light. The optical field coherently excites the long-lived noble-gas spins, which, in turn, alter the field, generating sharp complex-Lorentzian spectral lines. We model the coupling via hybridization of the noble-gas spins with the alkali spins and show that the magnetic field controls the degree of hybridization and thus the contrast and width of the optical lines. It is remarkable that the signal field is attenuated so efficiently by the mixture of alkali and noble-gas spins, despite each of them separately being transparent to light at the signal frequency. As this optical coupling exploits the long-lived coherence of the noble-gas spins, it could have various applications in precision measurements of magnetic or anomalous fields (*21*, *48*) and in the generation of long-lived entanglement and optical quantum memories for quantum sensing and quantum information processing (*32*, *35*).

MATERIALS AND METHODS

Detailed experimental configuration

We use an aluminosilicate spherical glass cell of diameter 14 mm containing 1500 torr of ^{3}He atoms and a droplet of potassium metal. The cell also contains 40 torr of N_2 gas for quenching and mitigation of radiation trapping. We use twisted-pair resistance wires with current oscillating at 450 kHz to stabilize the cell temperature to $T = 187$°C, yielding an estimated potassium density of $n_a \approx 8.5 \times 10^{13}$ cm^{-3}. A constant magnetic field $B\hat{z}$ is generated using a set of coils located within five layers of magnetic shields. The magnetic shields are degaussed and the transverse magnetic field is zeroed with an additional set of coils. The optical-pumping light originates from a single-mode, linearly polarized, distributed Bragg reflector (DBR) laser at 770 nm. It is amplified with a tapered amplifier and stabilized to 500 mW using a commercial noise eater and passes through a λ/4 retarder to render its polarization circular. The pumping light is blue-detuned from the D_1 optical line by 150 GHz and fills the entire cell (estimated beam waist diameter of 10 mm); these measures increase the spatial homogeneity of the alkali spin polarization.

We polarize the helium spins along $\hat{z}$ at a magnetic field of $B = 37$ mG using spin-exchange optical pumping. The EMF exerted by the helium on the potassium spins is built at a typical rate of 1 mG/hour, as measured by using the potassium as a magnetometer. The longitudinal lifetime of the helium spins is greater than 2.5 hours, plausibly limited by nonzero transverse magnetic field exerted by polarized helium atoms residing in the stem of the cell. The helium polarization is kept constant by a slow servo loop, which monitors the helium EMF, controls the pumping rate, and maintains the helium EMF at 2.8 mG to better than 1%. The decoherence rate of the helium spins $2\gamma_b = 4.8 \pm 1$ mHz is predominantly limited by spatial nonuniformity of the EMF of both species. To initialize each measurement with zero coherence of the collective helium spin, we apply a smooth pulse of magnetic-field gradient along $\hat{z}$. This dephases any precession of helium spin remnant from prior measurements due to its long coherence time.

The signal and control fields originate from another single-mode DBR laser at 770 nm. They are split using a polarizing beam splitter (PBS), sent to independent acousto-optic modulators, and the modulated beams are recombined using a second PBS. In the combined beam, the signal is typically 50 dB weaker than the control, and we vary the frequency difference between them (ω) through the relative radio frequencies of the two modulators. We use a retarder and a precision Soleil-Babinet compensator to align the linear polarization of the control field with the magnetic field. The input Gaussian beam, with 25 mW, is expanded to a waist of 7 mm and slightly focused to compensate for lensing by the spherical cell.

We measure the S_2 quadrature of the output beam $S_2^{out}(t)$ using a polarization heterodyne detection setup, comprising a zero-order λ/2 retarder at ~22. 5°, a PBS, and a differential photodetector. The detector outputs are subtracted and amplified, producing a readout proportional to $S_2^{out}(t)$. The exact angle of the retarder is set to null the readout in the presence of only the control field, i.e., to balance the detection. Digital Fourier transform is used to obtain $S_2^{out}(t)$. For normalization and for extraction of the phase shift $\varphi(\omega) = \arg [S_2^{out}(\omega)/S_2^{in}(\omega)]$, we also sample the input beam before the cell and measure $S_2^{in}(\omega)$ using a similar setup. To measure the optically excited nuclear spin precession after turning off the signal, we use the alkali spins as an effective magnetometer, probed by polarization rotation of the control field. The polarization rotation is linearly proportional

to $F_x(t)$, which, in turn, is proportional to the noble-gas spin $R_\perp(t)$ oscillating in the *xy* plane, as inferred from Eq. 11. This harmonic signal has an amplitude $R_{0\perp}(\Delta)$, which is plotted in Fig. 2C. The scale of $R_{0\perp}(\Delta)$ is normalized such that $R_{0\perp}(\Delta = 0) = 1$.

Fitting and calibrations

Frequency variables throughout the paper indicate angular frequencies, and Hz = 2π rad/s. We independently calibrate γ_a and $\omega_a(B)$ by measuring the precession of the potassium spins. We slightly tilt the spins by applying a short pulse of magnetic field along $\hat{y}$ and monitor their precession using polarization rotation measurements in the presence of the pumping field and the magnetic field $B\hat{z}$. A fit of the precession frequency to the linear function $\omega_a(B) = g_a(B - B_0^b)$ yields an estimate of the helium EMF B_0^b and the effective gyromagnetic ratio g_a = 592 Hz/mG of the potassium. The latter is slower than the gyromagnetic ratio of a free electron by a factor of q_a = 4.7, corresponding to an estimated potassium polarization of p_a = 70% in the regime of rapid potassium-potassium collisions [theoretically, $q_a = 2I + 1 = 4$ in the absence of such collisions or when p_a = 100%, and $q_a = 6$ for $p_a = 0$; see (*28*)]. From these precession measurements, we also infer the decoherence rate of the potassium spins at low magnetic fields $\gamma_a = 51 \pm 3$ Hz in the presence of both pumping and control light.

Theoretical model

The complex amplitude of the electric field of the combined control and signal field is given by $\boldsymbol{E} = \mathcal{E}_c\hat{z} + (e^{i\omega t}\mathcal{E}_+ + e^{-i\omega t}\mathcal{E}_-)\hat{y}$. Here, $\mathcal{E}_c$ is the amplitude of the control field, and $\mathcal{E}_+$ is the amplitude of the signal field at the entrance to the cell, where $\mathcal{E}_- = 0$. These amplitudes vary along the cell. We describe the signal field before and after the cell in terms of the Stokes parameters $S_2(t) + iS_3(t) = 2(\boldsymbol{E}\cdot\hat{z})^*(\boldsymbol{E}\cdot\hat{y})$ and their spectral representation $S_2(\omega) = \mathcal{E}_c^*\mathcal{E}_- + \mathcal{E}_c\mathcal{E}_+^*$ and $S_3(\omega) = i(\mathcal{E}_c\mathcal{E}_+^* - \mathcal{E}_c^*\mathcal{E}_-)$.

Effect of light on atoms

The equations of motion for the transverse mean spin components of the alkali and noble-gas atoms comprise the Faraday and spin-exchange Hamiltonians (*32*)

$$\partial_t\mathbf{F} = (\omega_a\mathbf{F} - J_a\mathbf{R})\times\hat{z} - \gamma_a\mathbf{F} + \bar{a}\,p_a S_3(t)\,\hat{y} \tag{2}$$

$$\partial_t\mathbf{R} = (\omega_b\mathbf{R} - J_b\mathbf{F})\times\hat{z} - \gamma_b\mathbf{R} \tag{3}$$

Here, **F** and **R** denote, respectively, the mean alkali and noble-gas spin vectors in the *xy* plane, which experience Larmor precession at frequencies ω_a and ω_b and are coupled by the unidirectional coherent spin-exchange rates $J_a = q_a\zeta n_b p_a/2$ and $J_b = \zeta n_a p_b/2$. These rates depend on the number densities n_a, n_b and on the degree of polarization $0 \le p_a, p_b \le 1$ of the alkali and noble-gas spins, respectively, and on $\zeta(q_a = 4.7) = 4\times10^{-15}$ cm^{3}s^{-1} (*38*). The symmetric (bidirectional) coupling rate in the bosonic representation is $J = \sqrt{J_a J_b}$ (*38*). The circularly polarized component $S_3(t)$ of the combined control and signal field exerts light-shift on the alkali spin. In the far-detuned limit $|\delta_e| \gg \gamma_e$, the light shift tilts the spin (predominantly its $\hat{z}$ component) around the $\hat{x}$ axis at a rate $\bar{a} = 2r_e c/(3q_a A\delta_e)$. Here, $r_e = 2.8\times10^{-13}$ cm is the electron radius, *c* is the speed of light, and *A* is the beam area.

Transforming the alkali and noble-gas spin vectors to a complex coherence representation in the rotating frame $\widetilde{F}(t) = \boldsymbol{F}(t)(\hat{x} + i\hat{y})e^{i\omega t}$ and $\widetilde{R}(t) = \mathbf{R}(t)(\hat{x} + i\hat{y})e^{i\omega t}$, we carry out the rotating-wave approximation and find, in the steady state $\partial_t\widetilde{F} = \partial_t\widetilde{R} = 0$

$$\widetilde{F} = \frac{i\bar{a}\,p_a S_3(\omega)}{\gamma_a - i\delta_a + \frac{J^2}{\gamma_b - i\delta_b}} \tag{4}$$

and

$$\widetilde{R} = \frac{-iJ_b\bar{a}\,p_a S_3(\omega)}{\gamma_a - i\delta_a}\,\frac{1}{\gamma - i\Delta} \tag{5}$$

Equation 4 describes the alkali coherence driven by the signal field (S_3 component). The coupling to the noble gas is manifested as a complex Lorentzian $J^2/(\gamma_b - i\delta_b)$ added to the denominator. For slowly varying frequencies $\omega \ll \omega_a$, the rate γ_a is free from spin-exchange relaxation due to alkali-alkali collisions (*28*). Here, the alkali spins adiabatically follow the spin precession of the noble-gas spins, constantly oriented along the effective magnetic field they experience; spin-exchange relaxation affects only the spin components transverse to this effective magnetic field.

In the limit $|\delta_a| \gg \gamma_a$ realized in the experiment, this additional complex-Lorentzian generates a Lorentzian Raman resonance with a narrow linewidth 2γ. The noble-gas spin coherence in Eq. 5 is excited by the alkali-spin mediator and dominated as well by a complex Lorentzian function, with the width 2γ (Eq. 1) and detuning $\Delta = \delta_b - J^2\delta_a/(\delta_a^2 + \gamma_a^2)$, as we measure for $|\delta_a| \gg \gamma_a$ (Fig. 2C).

Effect of atoms on light

The combined control and signal beam traversing the atomic medium experiences polarization rotation

$$S_2^{out}(\omega) = S_2^{in}(\omega) + \alpha\widetilde{F} \tag{6}$$

while $S_3^{out}(\omega) = S_3^{in}(\omega)$ remains constant. Here, $\alpha = dn_a\bar{a}AP_c/(4\hbar\omega_e)$, where P_c is the power of the control field and $\hbar\omega_e$ is the photon energy. Substituting the alkali coherence Eq. 4 in the limit $|\delta_a| \gg \gamma_a$ into Eq. 6 yields the optical spectral response

$$S_2^{out}(\omega) = S_2^{in}(\omega)\left(1 - \mathcal{C}_0\frac{\gamma}{\gamma - i\Delta}\right) \tag{7}$$

where

$$\mathcal{C}_0 = \frac{p_a\mathrm{OD}}{2}\,\frac{\gamma_a'}{\gamma_a}\,\frac{\gamma - \gamma_b}{\gamma} \tag{8}$$

is the amplitude of the complex Lorentzian. It depends on the hot, on-resonance optical depth (OD) and on the relaxation of the alkali spins due to scattering of control photons $\gamma_a' = \alpha\bar{a}/\mathrm{OD}$, with respect to the total relaxation rate γ_a. From Eq. 7, we obtain the phase shift

$$\varphi(\omega) \equiv \arg\frac{S_2^{out}(\omega)}{S_2^{in}(\omega)} = a\tan\left(\frac{\mathcal{C}_0\gamma\Delta}{\Delta^2 + \gamma^2(1 - \mathcal{C}_0)}\right) \tag{9}$$

and we find that $|S_2^{out}(\omega)/S_2^{in}(\omega)|^2$ is exactly an inverted Lorentzian, with width 2γ and contrast

$$\mathcal{C} = \mathcal{C}_0(2 - \mathcal{C}_0) \tag{10}$$

as presented in Fig. 2 (A and B).

For the experiments presented in Fig. 2 (C and D), the input signal field is turned off and the control field is kept on to act as a

monitor. The noble-gas spins precess at their bare frequency ω_b, and the alkali spins adiabatically follow. The x projection of the alkali spins, in a frame oscillating at a frequency ω_b, determines the rotation of the control field and is given by

$$F_x(t) = \frac{J_a}{\sqrt{(\omega_a - \omega_b)^2 + \gamma_a^2}} R_\perp(t) \quad (11)$$

where $R_\perp(t) = \mathrm{Re}[\mathbf{R}(t)(\cos\psi\hat{x} + i\sin\psi\hat{y})e^{i\omega_b t}]$ is the noble-gas projection, which depends on the parameter $\sin\psi = \gamma_a/\sqrt{(\omega_a - \omega_b)^2 + \gamma_a^2}$. At our moderate magnetic fields, in which the alkali is far detuned $|\omega_a - \omega_b| \gg \gamma_a$ (so that $\sin\psi \ll \cos\psi$), the measurement is predominantly sensitive to the x component of the noble-gas spins.

REFERENCES AND NOTES

1. B. C. Rose, D. Huang, Z. Zhang, P. Stevenson, A. M. Tyryshkin, S. Sangtawesin, S. Srinivasan, L. Loudin, M. L. Markham, A. M. Edmonds, D. J. Twitchen, S. A. Lyon, N. P. de Leon, Observation of an environmentally insensitive solid-state spin defect in diamond. *Science* **361**, 60–63 (2018).
2. S. Maity, L. Shao, S. Bogdanović, S. Meesala, Y. Sohn, N. Sinclair, B. Pingault, M. Chalupnik, C. Chia, L. Zheng, K. Lai, M. Lončar, Coherent acoustic control of a single silicon vacancy spin in diamond. *Nat. Commun.* **11**, 193 (2020).
3. D. Serrano, J. Karlsson, A. Fossati, A. Ferrier, P. Goldner, All-optical control of longlived nuclear spins in rare-earth doped nanoparticles. *Nat. Commun.* **9**, 2127 (2018).
4. D. Roy, C. M. Wilson, O. Firstenberg, Colloquium: Strongly interacting photons in one-dimensional continuum. *Rev. Mod. Phys.* **89**, 021001 (2017).
5. N. Bezginov, T. Valdez, M. Horbatsch, A. Marsman, A. C. Vutha, E. A. Hessels, A measurement of the atomic hydrogen Lamb shift and the proton charge radius. *Science* **365**, 1007–1012 (2019).
6. M. Sinhal, Z. Meir, K. Najafian, G. Hegi, S. Willitsch, Quantum-nondemolition state detection and spectroscopy of single trapped molecules. *Science* **367**, 1213–1218 (2020).
7. E. Oelker, R. B. Hutson, C. J. Kennedy, L. Sonderhouse, T. Bothwell, A. Goban, D. Kedar, C. Sanner, J. M. Robinson, G. E. Marti, D. G. Matei, T. Legero, M. Giunta, R. Holzwarth, F. Riehle, U. Sterr, J. Ye, Demonstration of 4.8×10^{-17} stability at 1 s for two independent optical clocks. *Nat. Photon.* **13**, 714–719 (2019).
8. M. S. Safronova, D. Budker, D. DeMille, D. F. Jackson Kimball, A. Derevianko, C. W. Clark, Search for new physics with atoms and molecules. *Rev. Mod. Phys.* **90**, 025008 (2018).
9. K. Hammerer, A. S. Sørensen, E. S. Polzik, Quantum interface between light and atomic ensembles. *Rev. Mod. Phys.* **82**, 1041–1093 (2010).
10. R. Shaham, O. Katz, O. Firstenberg, Quantum dynamics of collective spin states in a thermal gas. *Phys. Rev. A* **102**, 012822 (2020).
11. S. Kadlecek, T. Walker, D. K. Walter, C. Erickson, W. Happer, Spin-axis relaxation in spin-exchange collisions of alkali-metal atoms. *Phys. Rev. A* **63**, 052717 (2001).
12. I. Novikova, R. Walsworth, Y. Xiao, Electromagnetically induced transparency-based slow and stored light in warm atoms. *Laser Photon. Rev.* **6**, 333–353 (2012).
13. O. Firstenberg, M. Shuker, A. Ron, N. Davidson, Colloquium: Coherent diffusion of polaritons in atomic media. *Rev. Mod. Phys.* **85**, 941–960 (2013).
14. M. Klein, M. Hohensee, D. F. Phillips, R. L. Walsworth, Electromagnetically induced transparency in paraffin-coated vapor cells. *Phys. Rev. A* **83**, 013826 (2011).
15. M. V. Balabas, T. Karaulanov, M. P. Ledbetter, D. Budker, Polarized alkali-metal vapor with minute-long transverse spin-relaxation time. *Phys. Rev. Lett.* **105**, 070801 (2010).
16. W. Qu, S. Jin, J. Sun, L. Jiang, J. Wen, Y. Xiao, Sub-Hertz resonance by weak measurement. *Nat. Commun.* **11**, 1752 (2020).
17. D. Budker, V. Yashchuk, M. Zolotorev, Nonlinear magneto-optic effects with ultranarrow widths. *Phys. Rev. Lett.* **81**, 5788–5791 (1998).
18. O. Katz, O. Firstenberg, Light storage for one second in room-temperature alkali vapor. *Nat. Commun.* **9**, 2074 (2018).
19. T. W. Kornack, R. K. Ghosh, M. V. Romalis, Nuclear spin gyroscope based on an atomic comagnetometer. *Phys. Rev. Lett.* **95**, 230801 (2005).
20. T. G. Walker, M. S. Larsen, Spin-exchange-pumped NMR gyros. *Adv. At. Mol. Opt. Phy.* **65**, 373–401 (2016).
21. T. R. Gentile, P. J. Nacher, B. Saam, T. G. Walker, Optically polarized ^{3}He. *Rev. Mod. Phys.* **89**, 045004 (2017).
22. J. Lee, A. Almasi, M. V. Romalis, Improved limits on spin-mass interactions. *Phys. Rev. Lett.* **120**, 161801 (2018).
23. T. E. Chupp, P. Fierlinger, M. J. Ramsey-Musolf, J. T. Singh, Electric dipole moments of atoms, molecules, nuclei, and particles. *Rev. Mod. Phys.* **91**, 015001 (2019).
24. M. Smiciklas, J. M. Brown, L. W. Cheuk, S. J. Smullin, M. V. Romalis, New test of local lorentz invariance using a ^{21}Ne-Rb-K comagnetometer. *Phys. Rev. Lett.* **107**, 171604 (2011).
25. M. Bulatowicz, R. Griffith, M. Larsen, J. Mirijanian, C. B. Fu, E. Smith, W. M. Snow, H. Yan, T. G. Walker, Laboratory search for a long-range *T*-Odd, *P*-Odd interaction from axionlike particles using dual-species nuclear magnetic resonance with polarized ^{129}Xe and ^{131}Xe gas. *Phys. Rev. Lett.* **111**, 102001 (2013).
26. T. G. Walker, W. Happer, Spin-exchange optical pumping of noble-gas nuclei. *Rev. Mod. Phys.* **69**, 629–642 (1997).
27. M. Batz, P.-J. Nacher, G. Tastevin, Fundamentals of metastability exchange optical pumping in helium. *J. Phys. Conf. Ser.* **294**, 012002 (2011).
28. S. Appelt, A. Ben-Amar Baranga, C. J. Erickson, M. V. Romalis, A. R. Young, W. Happer, Theory of spin-exchange optical pumping of ^{3}He and ^{129}Xe. *Phys. Rev. A* **58**, 1412–1439 (1998).
29. T. W. Kornack, M. V. Romalis, Dynamics of two overlapping spin ensembles interacting by spin exchange. *Phys. Rev. Lett.* **89**, 253002 (2002).
30. A. Korver, D. Thrasher, M. Bulatowicz, T. G. Walker, Synchronous spin-exchange optical pumping. *Phys. Rev. Lett.* **115**, 253001 (2015).
31. Y. Zhan, X. Peng, S. Li, L. Zhang, J. Chen, H. Guo, Observation of transferred dressed spin effect via metastability-exchange collisions in ^{3}He atoms. *Appl. Phys. B* **125**, 170 (2019).
32. O. Katz, R. Shaham, E. S. Polzik, O. Firstenberg, Long-lived entanglement generation of nuclear spins using coherent light. *Phys. Rev. Lett.* **124**, 043602 (2020).
33. A. Dantan, G. Reinaudi, A. Sinatra, F. Laloe, E. Giacobino, M. Pinard, Long-lived quantum memory with nuclear atomic spins. *Phys. Rev. Lett.* **95**, 123002 (2005).
34. G. Reinaudi, A. Sinatra, A. Dantan, M. Pinard, Squeezing and entangling nuclear spins in helium 3. *J. Mod. Opt.* **54**, 675–695 (2010).
35. O. Katz, E. Reches, R. Shaham, A. V. Gorshkov, O. Firstenberg, Optical quantum memory with optically inaccessible noble-gas spins. arXiv:2007.08770 (2020).
36. O. Katz, R. Shaham, E. Reches, A. V. Gorshkov, O. Firstenberg, Optimal control of an ptical quantum memory based on noble-gas spins. arXiv:2007.10177 (2020).
37. D. Budker, W. Gawlik, D. F. Kimball, S. M. Rochester, V. V. Yashchuk, A. Weis, Resonant nonlinear magneto-optical effects in atoms. *Rev. Mod. Phys.* **74**, 1153–1201 (2002).
38. O. Katz, R. Shaham, O. Firstenberg, Quantum interface for noble-gas spins. arXiv:1905.12532 (2019).
39. O. Katz, O. Peleg, O. Firstenberg, Coherent coupling of alkali atoms by random collisions. *Phys. Rev. Lett.* **115**, 113003 (2015).
40. C. H. Volk, T. M. Kwon, J. G. Mark, Measurement of the ^{87}Rb-^{129}Xe spin-exchange cross section. *Phys. Rev. A* **21**, 1549–1555 (1980).
41. A. Weis, J. Wurster, S. I. Kanorsky, Quantitative interpretation of the nonlinear Faraday effect as a Hanle effect of a light-induced birefringence. *J. Opt. Soc. Am B* **10**, 716–724 (1993).
42. W. Gawlik, S. Pustelny, Nonlinear Faraday effect and its applications in horizons, in *World Physics: New Trends in Quantum Coherence and Nonlinear Optics* (Nova Science Publishers, 2009), vol. 263, pp. 45–82.
43. C. B. Moller, R. A. Thomas, G. Vasilakis, E. Zeuthen, Y. Tsaturyan, M. Balabas, K. Jensen, A. Schliesser, K. Hammerer, E. S. Polzik, Quantum back-action-evading measurement of motion in a negative mass reference frame. *Nature* **547**, 191–195 (2017).
44. R. A. Thomas, M. Parniak, C. Østfeldt, C. B. Moller, C. Bærentsen, Y. Tsaturyan, A. Schliesser, J. Appel, E. Zeuthen, E. S. Polzik, Entanglement between distant macroscopic mechanical and spin systems. arXiv:2003.11310 (2020).
45. E. Zeuthen, E. S. Polzik, F. Y. Khalili, Gravitational wave detection beyond the standard quantum limit using a negative-mass spin system and virtual rigidity. *Phys. Rev. D* **100**, 062004 (2019).
46. J. Sherson, A. S. Sørensen, J. Fiurášek, K. Mølmer, E. S. Polzik, Light qubit storage and retrieval using macroscopic atomic ensembles. *Phys. Rev. A* **74**, 011802(R) (2006).
47. C. A. Muschik, K. Hammerer, E. S. Polzik, J. I. Cirac, Efficient quantum memory and entanglement between light and an atomic ensemble using magnetic fields. *Phys. Rev. A* **73**, 062329 (2006).
48. I. M. Bloch, Y. Hochberg, E. Kuflik, T. Volansky, Axion-like relics: New constraints from old comagnetometer data. *J. High Energ. Phys.* **167**, 2020 (2020).

Acknowledgments: We thank M. Dikopoltsev and O. Tal for assistance in constructing the magnetic setup and setting the remote control, and C. Avinadav, R. Finkelstein, and O. Peleg for fruitful discussions. **Funding:** We acknowledge financial support by the Israel Science Foundation, the European Research Council starting investigator grant Q-PHOTONICS 678674, the Pazy Foundation, the Minerva Foundation with funding from the Federal German Ministry

for Education and Research, and the Laboratory in Memory of Leon and Blacky Broder. **Author contributions:** All authors contributed to the experimental design, construction, data collection, and analysis of this experiment. O.K. claims responsibility for Figs. 1 2, and 3. The authors wrote the manuscript together. **Competing interests:** The authors declare that they have no competing interests. **Data and materials availability:** All data needed to evaluate the conclusions in the paper are present in the paper. Additional data related to this paper may be requested from the authors.

Submitted 22 September 2020
Accepted 12 February 2021
Published 2 April 2021
10.1126/sciadv.abe9164

Citation: O. Katz, R. Shaham, O. Firstenberg, Coupling light to a nuclear spin gas with a two-photon linewidth of five millihertz. *Sci. Adv.* **7**, eabe9164 (2021).